

# TRANSITION TO A QUASI-FULLY DEVELOPED MHD FLOW IN AN ELECTRICALLY CONDUCTING PIPE UNDER A TRANSVERSE NON-UNIFORM MAGNETIC FIELD

Gautam Pulugundla,\* Sergey Smolentsev, Tyler Rhodes, Charlie Kawczynski and Mohamed Abdou

*Fusion Science & Technology Center, University of California, Los Angeles, USA*  
gautam@fusion.ucla.edu

*Interaction between liquid metal flows and non-uniform magnetic fields occurs in certain regions of fusion power reactors such as the breeding blanket access pipes. Here, the resulting high MHD pressure drop leads to numerous design challenges. Therefore, in this paper we perform numerical simulations to analyze the effect of a non-uniform transverse magnetic field on a liquid metal flow in a straight electrically conducting pipe. In particular, we perform parametric analyses at different conductance ratios and magnetic interaction parameters to quantify their effect on MHD pressure drop in pipes. The results also help in establishing a range for the control parameters in which the flow transforms from a quasi-fully developed to a fully three-dimensional state.*

## I. INTRODUCTION

Eutectic alloy lead-lithium (PbLi, liquid metal) is used in breeding blankets of a fusion power reactor, such as DCLL (dual-coolant lead-lithium), HCLL (helium-cooled lead lithium) and SCLL (self-cooled lead lithium), as coolant and breeder. However, PbLi being electrically conducting, when exposed to the plasma-confining magnetic field, experiences strong magnetohydrodynamic (MHD) effects.<sup>1,2</sup> One such MHD effect is the interaction between the flowing PbLi and a non-uniform (fringing) magnetic field in the inlet and outlet pipes connected to the blanket manifold. When the liquid metal interact with such spatially varying magnetic field, strong 3D electric currents are induced which may result in intolerably high MHD pressure drops. It is therefore very important to characterize and quantify this interaction for the accurate design of any PbLi based breeding blanket.

Earlier experimental and numerical studies focused on understanding this MHD interaction through the use of simplified numerical formulations,<sup>3-7</sup> experiments and full three dimensional simulations.<sup>8-11</sup> However, most of them were restricted to either to uniform magnetic fields or to just a specific set of control parameters. Therefore, in this work we endeavor to perform a parametric study by considering a liquid metal flow in a pipe with electrically conducting walls under the influence of a fringing transverse magnetic field using the wall conductance ratio, flow velocity, magnetic field gradient

and strength as control parameters. In particular, we consider the case of a flow entering the magnetic field. The numerical method based on the MHD code HIMAG is employed for the simulations. Studies performed by Refs. 12 and 13 suggest that under certain conditions the MHD pressure drop can be estimated through the use of a so-called quasi-fully-developed (QFD) flow assumption. This assumption is very simple to implement and is known to perform well provided the quasi-two-dimensional (Q2D) assumption is valid.<sup>3</sup> However, a systematic parametric investigation has never been performed to verify the extent of validity of the QFD assumption. Therefore, the particular focus of this work is on characterization of flow transition to a quasi-two-dimensional from a fully three-dimensional flow for the range of control parameters through the evaluation of the axial and transverse pressure gradients.

## II. PROBLEM DEFINITION

### II.A. Geometry

We consider the flow of an isothermal, viscous, incompressible and electrical conducting fluid (liquid metal) in a pipe with electrically conducting and non-magnetic walls, as sketched in Fig. 1.

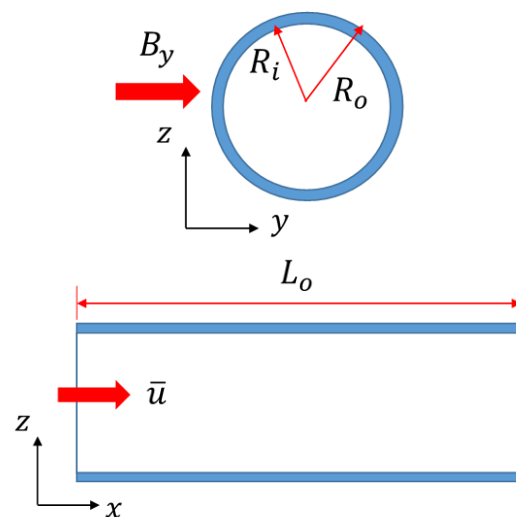


Fig. 1. Schematic illustrating the flow geometry.

The pipe is characterized by its inner radius  $R_i$ , outer radius  $R_o$  and length  $L_o$ . For this configuration we study the interaction of the flow in the x-direction with a non-uniform magnetic field  $B(x)$  imposed in the transverse y-direction. The entry effects of the flow into the region of the magnetic field and its subsequent impact on the MHD pressure drop is the object of our investigation. For the ease of parameterization, we characterize the fluid flow and the magnetic field using the following well-known non-dimensional control parameters, starting with the Reynolds number

$$Re = \frac{\rho \bar{u} R_i}{\mu}, \quad (1)$$

Hartmann number

$$Ha = B_{max} R_i \sqrt{\frac{\sigma_f}{\mu}}. \quad (2)$$

Here  $\bar{u}$ ,  $B_{max}$ ,  $\rho$ ,  $\mu$ ,  $\sigma_f$  are mean flow velocity, maximum magnetic field, fluid density, dynamic viscosity, and fluid electric conductivity, respectively. The effect of both Reynolds and Hartmann numbers can be expressed through the non-dimensional interaction parameter,

$$N = \frac{Ha^2}{Re}. \quad (3)$$

The final control parameter of interest in this study is the wall conductance ratio, given by

$$C_w = \frac{\sigma_w (R_o^2 - R_i^2)}{\sigma_f (R_o^2 + R_i^2)}. \quad (4)$$

Here,  $\sigma_w$  is the wall electric conductivity. We should mention here that throughout the present work, we assume that the magnetic Reynolds number is negligibly small ( $Re_m = \mu_0 \sigma_f R_i \bar{u} \ll 1$ ).<sup>14</sup> This assumption is justified for most liquid metal flows. The consequence of this idealization is that the imposed magnetic field does not change under the influence of the fluid flow.

Following such a *quasi-static* assumption the eddy currents induced in the liquid metal can be expressed through Ohm's law as:

$$\vec{j} = -\nabla\varphi + (\vec{u} \times \vec{B}). \quad (5)$$

Here,  $\vec{u}$  (here in vector notation) is the fluid velocity vector,  $\vec{B}$  is the unperturbed magnetic field vector and  $\varphi$  is the electric scalar potential. Combining this with charge conservation  $\nabla \cdot \vec{j} = 0$ , we get the governing Poisson equation for the electrical potential:

$$\nabla^2 \varphi = \nabla \cdot (\sigma_r \vec{u} \times \vec{B}). \quad (6)$$

Here,  $\sigma_r$  is the spatially varying electrical conductivity normalized using the liquid metal conductivity. The Poisson equation is coupled with the Navier–Stokes equations (in the non-dimensional form) through the Lorentz force density acting a volume source in the momentum equation:

$$\frac{\partial \vec{u}}{\partial t} + (\vec{u} \cdot \nabla) \vec{u} = -\nabla p + \frac{1}{Re} \nabla^2 \vec{u} + \frac{Ha^2}{Re} (\vec{j} \times \vec{B}), \quad (7)$$

$$\nabla \cdot \vec{u} = 0, \quad (8)$$

We determine the velocity field  $\vec{u}(\vec{x}, t)$ , pressure field  $p(\vec{x}, t)$ , electric potential  $\varphi(\vec{x}, t)$ , and the electric current density  $\vec{j}(\vec{x}, t)$ , from Eqs. (6) – (8) using the following boundary conditions:  $n \cdot \vec{j} = 0$  on all the boundaries (implies that  $\partial\varphi/\partial n = 0$ ) including the inlet and outlet,  $\partial\vec{u}/\partial n = 0$  and  $p = 0$  at the outlet (where  $n$  is the vector normal) and a no-slip condition at the fluid-wall interface. The velocity field corresponding to the

laminar hydrodynamic pipe flow,  $\vec{u} = 2\bar{u} \left( 1 - \frac{r^2}{R_i^2} \right) \cdot \hat{e}_x$  is imposed at the inlet of the flow domain.

Here  $r$  represents the radial coordinate.

## II.B. Magnetic Field Distribution

The fringing magnetic field required for the calculation can be assumed to be produced by a magnetic system of fixed length such that its front edge is located at a streamwise position  $x_s$ . The liquid metal flows in an electrically conducting pipe from left to right (Fig. 2.) and enters this transverse magnetic field.

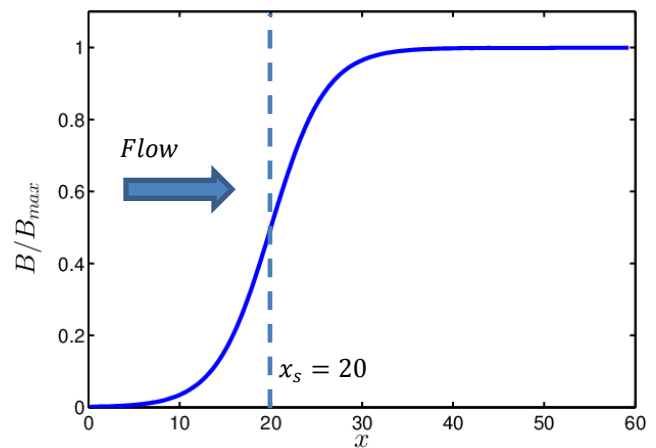


Fig. 2. Non-uniform magnetic field distribution inside the electrically conducting pipe.

For such a configuration, the magnetic field distribution is given by:

$$\frac{\vec{B}}{B_{max}} = \frac{1}{2} \left[ 1 + \tanh \left( \frac{x-x_s}{\beta} \right) \right] \cdot \widehat{e}_y, \quad 0 \leq \frac{x}{L_0} \leq 1. \quad (9)$$

Here,  $\widehat{e}_y$  represents the unit vector in the  $y$ -direction,  $\beta$  is the parameter that controls the magnetic field gradient. The smaller the value of  $\beta$  the stronger the gradient. In order to help with the parametric study, we represent this gradient through an additional new non-dimensional parameter called the gradient Hartmann number as,

$$Ha_G = \left( \frac{\partial B}{\partial x} \right)_{x_s} R_i^2 \sqrt{\frac{\sigma_f}{\mu}} \quad (10)$$

Here,  $\left( \frac{\partial B}{\partial x} \right)_{x_s}$  represents the gradient of the magnetic field and the subscript denotes the location,  $x_s$  at which this gradient is evaluated as shown in Fig. 2. From a theoretical standpoint  $Ha_G$  can be understood as a quantity that represents the effect of electromagnetic forces arising from the axial component of electric currents that are generated due to the fringing magnetic field. This is unlike the normal Hartmann number that embodies the effect of cross-sectional currents as a result of a uniform magnetic field in fully developed MHD flows. Therefore,  $Ha_G$  together with the normal  $Ha$  encompass the three-dimensional nature of the currents and associated 3D pressure drop for MHD flows in fringing magnetic fields. As can be seen in Eq. 9, in this study we only consider one component of the magnetic field. This is because of the negligible contribution of the other two components to the overall pressure drop in pipes. This was demonstrated in Ref. 13 through full computations involving all magnetic field components based on a curl and divergence free condition.

### III. NUMERICAL METHOD

The numerical solver employed in this work is called HIMAG.<sup>15</sup> It is a 3D finite volume CFD code developed by HyPerComp, Inc., in collaboration with UCLA especially for MHD flows at low magnetic Reynolds number in fusion applications. HIMAG utilizes an algorithm based on MPI parallelization for distributed memory computations. The numerical method involved the use of a discretization scheme based on a collocated grid arrangement where the all the flow variables are stored at the cell centers. The convective and diffusive terms of the momentum equation (Eq. 7) are discretized using a semi-implicit Crank-Nicholson formulation, and a four step projection method is used for the hydrodynamic solver of HIMAG. The electric potential Poisson equation

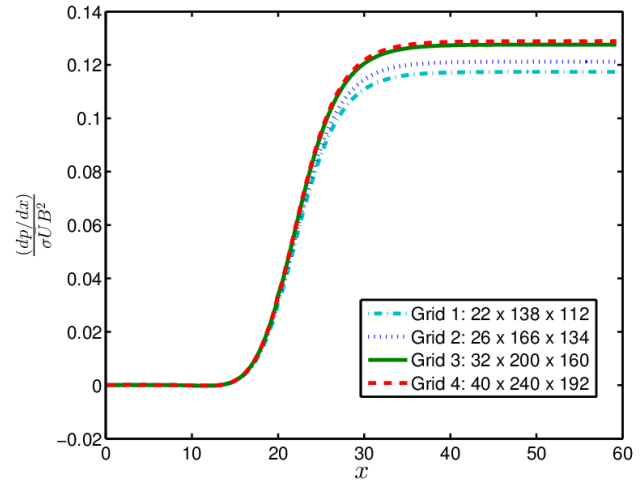


Fig. 3. Non-dimensionalized axial pressure gradient along the  $x$ -direction at  $N = 45$ ,  $C_w = 0.15$ . The numerical results are plotted for increasing grid sizes in radial, azimuthal and axial directions, respectively as a part of grid sensitivity study.

(Eq. 6) is solved to calculate the Lorentz force density ( $\vec{J} \times \vec{B}$ ) required to the close the Navier-Stokes equations.

For the present geometry of a pipe, we use the in-built structural grid generator of HIMAG to produce a non-uniform mesh in both the fluid and solid wall regions where the governing equations are solved. In particular, non-uniform mesh in the radial direction is employed with 5 cells in the Hartmann boundary layer to completely resolve the flow gradients. The grid in the azimuthal direction is maintained uniform. Axially, the mesh is more refined in the fringing magnetic field region where the gradient of the magnetic field is strongest. In total, we employ a grid with 32, 200 and 160 grid points in radial, azimuthal and axial directions, respectively. Finally, the mesh inside the solid wall contains 5 grid points in the radial direction.

In order to ensure the accuracy of the numerical computations, we chose that particular grid based on grid sensitivity studies. These studies are performed using a series of grid sizes at progressively higher resolutions and by monitoring the variation of non-dimensional axial pressure gradient along the flow direction with each subsequent grid. The grid size that corresponds to an asymptotic numerical solution is eventually employed for the parametric studies (see Fig. 3).

### IV. RESULTS AND DISCUSSION

In this section we present the results from the parametric studies performed with the non-uniform magnetic field. For the ease of discussion we divided the study into sub-sections based on the parameter being considered. In particular, we analyze the effect of gradient Hartmann number, interaction parameter and the

conductance ratio on the transition from a QFD state to a three dimensional flow.

**IV.A. Effect of Magnetic Field Gradient**

We start our discussion by analyzing the effect of magnetic field gradient on the generation of strong 3D flow characteristics. These 3D effects are highly localized and are caused by the axial component of the induced electric current ( $J_x$ ) in the region of fringing magnetic field. As can be seen in Fig. 5c,  $J_x$  is in opposite directions in the upper and lower half of  $xz$  flow cross-section.

Consequently, the Lorentz force density component is normal to the applied magnetic field and points to the center of the flow domain. This action of the Lorentz force moves the fluid away from the walls parallel to the magnetic field and pushes it to the core of the pipe. This

results in the lowest fluid pressure locally adjacent to those walls. Upon entering the region of the uniform magnetic field, however, the Lorentz forces acts as expected along the streamwise direction thereby deforming the initially laminar hydrodynamic flow into the well-known M-shaped velocity profile with side wall high velocity jets as seen in Figs.5a and 5b.

We will now quantify the action of the fringing field by comparing the axial pressure gradients at two different cross-sectional locations. It is well known that when the flow is fully or even QFD there would be a uniform pressure distribution in the pipe cross-section. Any deviation from such a uniformity indicates the generation of an axial eddy current density component leading to a transverse Lorentz force. The onset of this 3D effect of the fringing magnetic field can be quantified by evaluating the difference in the axial pressure gradients

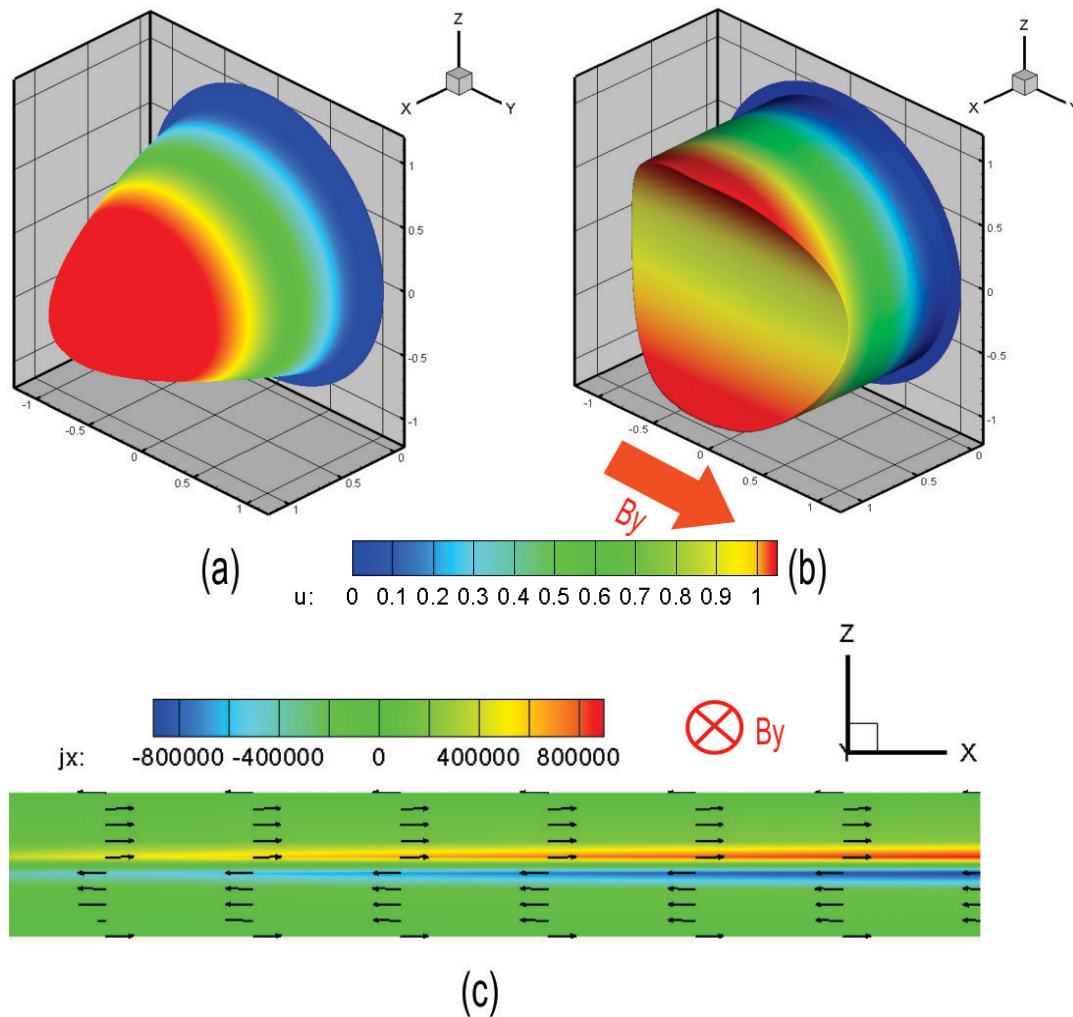


Fig. 5. The figure illustrates, (a), (b) the streamwise velocity profile in the regions without and with a magnetic field, respectively, and (c) the induced electric current distributions in the central plane normal to the magnetic field. These axial eddy currents  $j_x$  are generated due to the fringing magnetic field. Data is from the simulation that is performed at  $Ha_G = 583.34$ ,  $Re = 2000$ ,  $Ha = 1500$  and  $C_w = 0.03$ ,

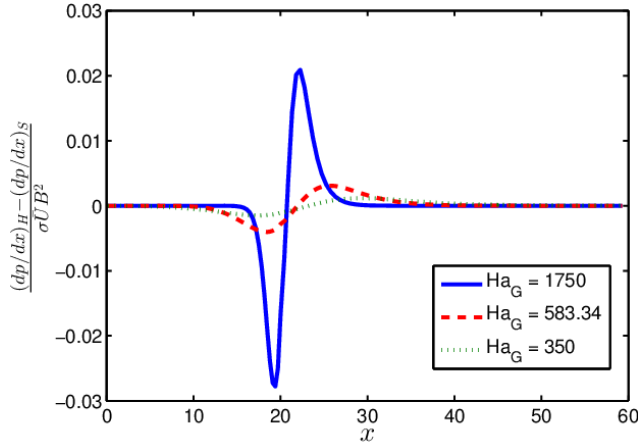


Fig. 6. Difference in non-dimensionalized axial pressure gradient in the boundary layers both perpendicular and parallel to the magnetic field. The results are illustrated for different gradient Hartmann numbers  $Ha_G$  at  $N = 45$  and  $C_w = 0.03$ .

between walls perpendicular  $(dp/dx)_H$  and parallel  $(dp/dx)_S$  to the magnetic field. We perform this analysis for three different gradient Hartmann numbers ( $Ha_G$ ). As shown in Fig. 6, flows at all the three  $Ha_G$  demonstrate a fully developed state in the uniform magnetic field regions towards the inlet ( $\vec{B} = \mathbf{0}$ ) and outlet ( $\vec{B} = \mathbf{B}_{max} \cdot \hat{e}_y$ ) of the pipe.

In the fringing region, however, all these regimes deviate from the fully/quasi-fully developed state. The strongest of this deviation can be observed at  $Ha_G = 1750$  as illustrated by the two peaks in the transverse pressure gradient difference in Fig. 6. This is purely due to the sharp magnetic field gradient in the fringing region.

#### IV.B. Effect of Interaction Parameter

From the above analysis it is apparent that all the 3D effects are confined to a much localized region inside the pipe. Therefore, in terms of blanket manifold design it would be highly useful to analyze if the MHD pressure drop can still be approximated using the simple analytical expression for QFD flows. Therefore, in the following sections we endeavor to understand and quantify the effect of 3D flow behavior on the MHD pressure gradient in the pipe for different interaction parameters and conductance ratios.

We start our analysis with the interaction parameter (Eq. 3). Interaction parameter is one of the most important non-dimensional parameters associated with fusion MHD flows as it encompasses the effect of both Hartmann and Reynolds numbers. Therefore, in this work, we performed simulations at a Reynolds number pertaining to a purely “laminar” state ( $Re = 2000$ ) and varied the Hartmann number so as to analyze the effect of the interaction parameter on flow transition from QFD to a 3D state. This

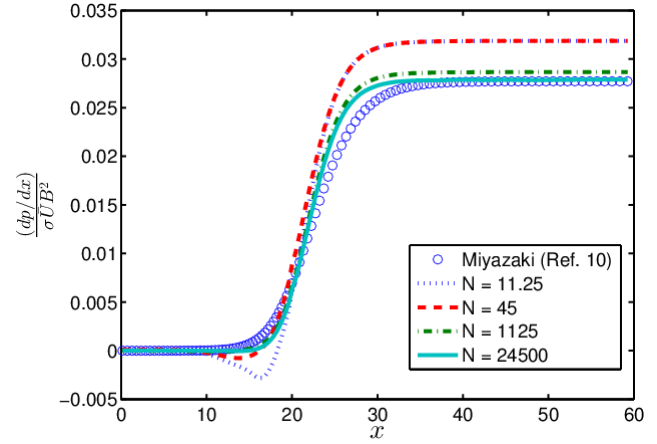


Fig. 7. Non-dimensionalized axial pressure gradient along the  $x$ -direction. The results are illustrated for different interaction parameters  $N$  at  $Ha_G = 583.34$  and  $C_w = 0.03$ . The numerical results (lines) are compared with those obtained the Miyazaki formula (symbols).<sup>12</sup>

procedure further helps in avoiding flows where a turbulent flow state could theoretically be present for some distance into the entrance of the pipe before the magnetic field.

For the analysis, we compare the axial pressure gradient at the middle of the pipe from the numerical simulations with those obtained theoretically (Eq. 10) using the QFD flow assumption of Ref. 12.

$$\frac{dp}{dx} = \frac{C_w}{1+C_w} \sigma_f \bar{u} B^2(x). \quad (11)$$

As can be observed from Fig. 7, at the highest interaction parameter of  $N = 24500$  both the theoretical and numerical simulations produce identical results in the uniform magnetic field region. There is, however, a slight difference in the fringing region owing to the 3D effects that are generated at the gradient Hartmann number of 583.34.

At smaller interaction parameters there is a disagreement between numerical and theoretical pressure gradient even in the uniform magnetic field region. This could be due to the fact that the analytical expression Eq. 10 neglects the flow inertia. In spite of this seemingly strong disagreement between both the results, it is still interesting to note that the MHD pressure can be estimated using the QFD assumption for fusion relevant flows at high  $N$ . This reiterates the fact that at high  $N$ , the contribution of inertia effects to the overall pressure losses is indeed negligible.

#### IV.C. Effect of Conductance Ratio

The final parameter of interest in our study is the conductance ratio  $C_w$ . To understand its effect on the

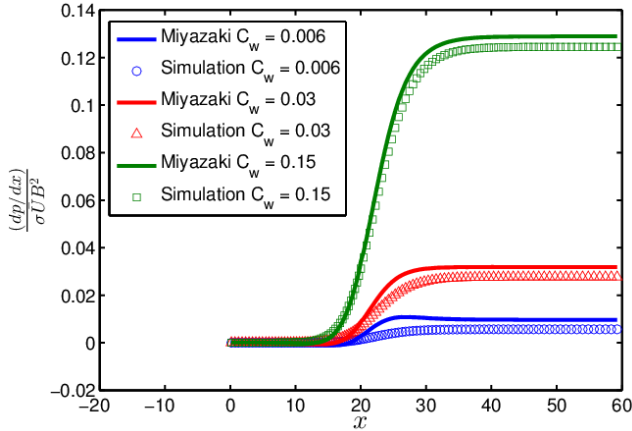


Fig. 8. Non-dimensionalized axial pressure gradient along the  $x$ -direction. The results are illustrated for different conductance ratios  $C_w$  at  $Ha_G = 583.34$  and  $N = 45$ . The numerical results (symbols) are compared with those obtained the Miyazaki formula (lines).<sup>12</sup>

pressure distribution in the pipe, we perform simulations for three different value of  $C_w$ .

The axial pressure gradient from the results of these simulations is again compared with those obtained from Eq. 10 at the middle of the duct. It is well known that with increase in conductance ratio, the overall pressure losses in the pipe also increase. This behavior can be clearly observed in the results illustrated in Fig. 8.

The interesting aspect, however, is the fact that the agreement between QFD flow assumption and numerical results in the fringing region gets better with increasing  $C_w$ . This could be due to the velocity redistribution which leads to a reduction in the flow velocity at the center of the pipe as the flow enters the region of the varying magnetic field. The higher core velocity at lower conductance ratios further produce stronger inertia effects which are neglected in Eq. 10.

## V. CONCLUSIONS AND FUTURE WORK

We performed parametric studies for a liquid metal flow entering a transverse non-uniform magnetic field. The computations illustrated clear trends in the variation of pressure gradient with respect to various control parameters. In particular, the following observations were made:

- For the assumed magnetic field distribution, the gradient of the fringing magnetic field has a strong influence on the transition to three-dimensionality
- The simple analytical equation for the MHD pressure drop based on the quasi-fully-developed MHD flow assumption<sup>10</sup> agrees well with the numerical simulations for the following conditions:
  - a. At high interaction parameters in both the fringing and fully developed region
  - b. At higher conductance ratio in the fringing magnetic field region

Our investigations could be extended to involve cases with a larger range of control parameters. This would be interesting as the results from that study could provide an exact scaling behavior of MHD pressure drop thereby paving the way for any future work on liquid metal breeding blanket design.

## ACKNOWLEDGMENTS

This study is supported by the U.S. Department of Energy, Office of Science, Office of Fusion Energy Sciences, under Award Number DE-FG02-86ER52123. The authors would like to thank Peter Huang from Hypercomp, Inc., for help with HIMAG. This work used computational and storage services associated with the Hoffman2 Shared Cluster provided by UCLA Institute for Digital Research and Education's Research Technology Group.

## REFERENCES

1. S. SMOLENTSEV et al., *Fusion Eng. Des.*, **83**, 5-6, 771 (2008); <http://dx.doi.org/10.1016/j.fusengdes.2008.07.023>.
2. S. SMOLENTSEV et al., *Fusion Eng. Des.*, **85**, 7-9, 1196 (2010); <http://dx.doi.org/10.1016/j.fusengdes.2010.02.038>.
3. R.J. HOLDROYD and J.S. WALKER, *J. Fluid Mech.*, **84**, 3, 471 (1978); <http://dx.doi.org/10.1017/S0022112078000282>.
4. B.F. PICOLOGLOU et al., *Fusion Technol.*, **10**, 3, 71 (1986).
5. C.B. REED et al., "ALEX Results – A Comparison of Measurements from a Round and a Rectangular Duct with 3-D Code Predictions," Proceedings of 12th Symposium on Fusion Engineering, Monterey, CA, October 12–16, 1987.
6. H. MADARAME and H. TOKOH, *J. Nucl. Sci. Technol.*, **25**, 4, 323 (1988); <http://dx.doi.org/10.1080/18811248.1988.9733596>.
7. X. ALBETS-CHICO et al., *Phys. Fluids*, **23**, 047101 (2011); <http://dx.doi.org/10.1063/1.3570686>.
8. L. BÜHLER and C. MISTRANGELO, *Fusion Eng. Des.*, **88**, 9-10, 2314 (2013); <http://dx.doi.org/10.1016/j.fusengdes.2013.03.009>.
9. Y. LI and O. ZIKANOV, *Fusion Eng. Des.*, **88**, 4, 195 (2013); <http://dx.doi.org/10.1016/j.fusengdes.2013.01.087>.
10. X. ALBETS-CHICO et al., *Fusion Eng. Des.*, **88**, 12, 3108 (2013); <http://dx.doi.org/10.1016/j.fusengdes.2013.09.002>.
11. O. ZIKANOV et al., *Appl. Mech. Rev.*, **66**, 3, 030802-1 (2014); <http://dx.doi.org/10.1115/1.4027198>.
12. K. MIYAZAKI et al., *J. Nucl. Sci. Technol.*, **28**, 2, 159 (1991); <http://dx.doi.org/10.1080/18811248.1991.9731336>.
13. F.-C. Li et al., *Fusion Eng. Des.*, **88**, 3060 (2013); <http://dx.doi.org/10.1016/j.fusengdes.2013.08.006>.
14. P. A. DAVIDSON, *An Introduction to Magnetohydrodynamics*, p. 119, Cambridge University Press, Cambridge (2001); <http://dx.doi.org/10.1017/CBO9780511626333>.
15. R. MUNIPALLI et al., DOE Phase-II SBIR, period of performance: June 2001–June 2003, Final Report (2003).